A numerical strategy to compute optical parameters in turbulent flow. Application to telescopes

Ramon Codina[1,*], Joan Baiges[1], Daniel Pérez-Sánchez[1] and Manuel Collados[2]

[1] International Center for Numerical Methods in Engineering (CIMNE),
Universitat Politècnica de Catalunya, Jordi Girona 1-3, Edifici C1, 08034 Barcelona, Spain.
[2] Instituto de Astrofísica de Canarias, Via Láctea s/n, 38205 La Laguna, Tenerife, Spain.
[*] ramon.codina@upc.edu

Contents

Abstract

We present a numerical formulation to compute optical parameters in a turbulent air flow. The basic numerical formulation is a large eddy simulation (LES) of the incompressible Navier-Stokes equations, which are approximated using a finite element method. From the time evolution of the flow parameters we describe how to compute statistics of the flow variables and, from them, the parameters that determine the quality of the visibility. The methodology is applied to estimate the optical quality around telescope enclosures.

1 Introduction

In spite of its impact in some applications, the problem of estimating the optical properties in a turbulent flow is not particularly popular in the computational fluid dynamics (CFD) community. An example where this problem is of paramount importance is in the determination of the location where large telescope facilities have to be built. The purpose of this paper is precisely to explain the problem and to propose a numerical formulation to approximate it.

The location for the construction of a telescope depends on several factors, some of them of logistic nature (such as the ease of construction or the scientific and political environment) and others, obviously, directly relevant to the quality of the astronomical observation. Among the latter, periods of good visibility (without clouds), weather conditions or the proximity to the Equator (leading to the so called sky quality) have an obvious impact. However, at least as important as those are the optical properties of the environment where the telescope enclosure is placed, primarily determined by the aerodynamic behavior of this enclosure.

The effect of the air dynamics around the telescope building on the visibility is due to the wave nature of light. Light rays, as the visible portion of the electromagnetic spectrum, travel at the light speed and with a wavelength between 400 and 800 nanometers in the vacuum. However, when they enter a transparent medium, such as the earth atmosphere, they decrease their speed, therefore changing their wavelength (the frequency is kept). The ratio between the speed of light in the vacuum and in a medium is the so called refractive index of this medium, that we will denote as usual by n.

For a single beam of light, if this beam is not orthogonal to the medium interface, refraction occurs. In a medium in which the refractive index changes from point to point, the direction of the beam of light suffers continuous changes. However, the problem arises when different light rays forming a wavefront enter a medium with variable refractive index. The variability of this index causes the different rays to refract in a different way, thus leading to wavefront distortion and a deterioration of the quality of the visibility.

The problem thus is the variability of the refractive index in the atmosphere rather than the refractive index itself. Here is where turbulence comes into the picture. Turbulence fluctuations, particularly in temperature, induce fluctuations in the refractive index that lead to visibility deterioration.

A first and classical approach to determine the feasibility of a certain site as a telescope location has been to quantify turbulence in the region, usually by experimental means. Classical turbulence parameters, such as the integral length, turbulence intensity or turbulence energy spectra have proved to be useful to assess the quality of a site to build a telescope. However, arguments derived from this information are merely qualitative, giving for granted that the higher the turbulence effects, the lower the visibility quality.

That CFD may play a role in this problem is obvious from what has been explained. The idea would simply be to replace experimental data by results of numerical simulations. In fact, the qualitative link between turbulence and optical quality led the International Center for Numerical Methods in Engineering (CIMNE) to participate in several projects related to the aerodynamic analysis of telescope buildings in collaboration with the Astrophysical Institute of the Canary Islands (IAC). In particular,

CIMNE has been involved in the aerodynamic analysis of the GTC telescope [12] and in the ELT project from the European Commission [10], as well as in the analysis of the ATST project of a solar telescope [1]. In this last case we have considered the possibility to go further, and to quantify the effect of turbulence in the visibility quality rather than simply computing the turbulence parameters.

In the astrophysical community, optical quality is measured, among other parameters, by the so called Fried parameter r_0 and the Greenwood frequency f_G (see [3, 22, 24] for background in the optical concepts to be used). Roughly speaking, the former corresponds to the diameter of a circle where the mean distortion expected of a light wavefront is 1 radian, whereas the latter gives an idea of the temporal frequency at which refraction varies. Both are essential in adaptive optics in astronomy. They are used to design segmented telescopes (the size of the segments being determined by the Fried parameter) and their actuators in typical active control systems of these devices.

The question is whether r_0 and f_G can be computed or not. If one assumes that the air flow is fully turbulent, the answer is positive. For length scales in the inertial range of the Kolmogorov energy cascade, it turns out that these parameters can be expressed in terms of the structure function of the refractive index and, under an isotropy assumption, by the square of the so called constant of structure, C_n^2 . This is, therefore, the scalar field that needs to be computed which, according to the previous discussion, must be related to the turbulence fluctuations. This dependence can be finally expressed as a relationship between C_n^2 and the mean pressure and the constant of structure of the temperature, which, in turn, depends on the gradients of the mean temperature and mean velocities. The conclusion is thus clear: If we are able to compute mean flow quantities (pressure, temperature and velocity) in a fully developed turbulent flow, we will be able to estimate the constant of structure of the refractive index and, from integration along the optical path of the light beam, the Fried parameter and the Greenwood frequency. These parameters need to be computed for all directions of observation of interest.

Once the model to compute the optical parameters is established (and accepted) the success depends on the CFD simulation to obtain mean flow quantities. However, now they are needed not only to establish a mere qualitative indication of the optical quality, but to compute a quantitative measure of this quality. The first and essential point to consider is that all the expressions to be used are derived under the assumption that the flow lies within the inertial range. The classical statistical temporal and spatial correlations between velocity components, pressure and temperature need to apply. This excludes from the very beginning the use of RANS (Reynolds averaged Navier-Stokes) models and restricts the alternatives to, at least, LES (large eddy simulation) formulations.

As basic numerical formulation for the aerodynamic problem we have used a stabilized finite element method for the spatial discretization together with a second order time integration scheme. The Smagorinsky model has been used as LES formulation, even though richer dynamics and still genuine turbulent behavior are obtained if the stabilization alone is let to act as turbulence model. Both the numerical formulation and the LES model are described in Section 2. Once the flow variables are computed and time averaged, the square of the constant of structure of the refractive index can be obtained. From these results one may now compute the Fried parameter and the Greenwood frequency by integration of functions that depend on C_n along different optical paths corresponding to the directions of observation of interest. A detailed description of how to perform these calculations is presented in Section 3.

As an example of application of the strategy presented, we have applied it to the ATST telescope mentioned earlier in Section 4. We believe this example may serve to understand the potential of CFD in the field of the optical environmental quality, which in the case of telescopes is crucial to select the site of these scientific installations. Some concluding remarks close the paper in Section 5.

2 The aerodynamic problem

2.1 Problem statement

In this section we shall consider the flow problem for an incompressible fluid taking into account the coupling of the Navier-Stokes equations with the heat transport equation through Boussinesq's assumption, as well as a nonlinear viscosity dependence on the velocity gradient invariants through Smagorinsky's LES model. Some comments will be made later on about the possibility to avoid turbulence modeling and to rely only on the numerical formulation.

The equations describing the problem are

$$\partial_t \boldsymbol{u} + (\boldsymbol{u}\cdot\nabla)\boldsymbol{u} - 2\nabla\cdot[\nu\boldsymbol{\varepsilon}(\boldsymbol{u})] + \nabla p + \beta\boldsymbol{g}\vartheta = \boldsymbol{f}, \tag{1}$$

$$\nabla\cdot\boldsymbol{u} = 0, \tag{2}$$

$$\partial_t\vartheta + (\boldsymbol{u}\cdot\nabla)\vartheta - \nabla\cdot(\kappa\nabla\vartheta) = 0, \tag{3}$$

to be solved in $\Omega\times(0,t_{\rm fin})$, where $\Omega\subset\mathbb{R}^3$ is the computational domain and $[0,t_{\rm fin}]$ is the time interval to be considered. In (1)-(3), $\boldsymbol{u}$ denotes the velocity field, p is the kinematic pressure (i.e., the pressure divided by the density), ϑ is the temperature, ν is the total kinematic viscosity (physical plus turbulent), $\boldsymbol{\varepsilon}(\boldsymbol{u})$ is the symmetrical part of the velocity gradient, β is the thermal expansion coefficient, $\boldsymbol{g}$ is the gravity acceleration vector, $\boldsymbol{f}$ is the vector of body forces, and κ is the total thermal diffusivity (that is, the physical plus turbulent thermal conductivity divided by the heat capacity). The density ρ_0 is assumed constant to obtain equations (1)-(3). In the numerical example of Section 4, all these properties have been taken as those corresponding to air in normal conditions.

The force vector $\boldsymbol{f}$ in (1) contains the reference buoyancy forces from Boussinesq's assumption, that is

$$\boldsymbol{f} = \boldsymbol{g}(1+\beta\vartheta_0).$$

In this equation, ϑ_0 is the reference temperature from which buoyancy forces are computed.

Smagorinsky's turbulence model has been employed in the numerical simulations (see, e.g. [20, 23, 9] for background). This model is tight to the numerical discretization in space of the flow equations, which in our case is performed using the finite element method. The turbulent kinematic viscosity associated to this model is

$$\nu_{\rm tur} = \rho_0^{-1} c h^2 \left[\boldsymbol{\varepsilon}(\boldsymbol{u}) : \boldsymbol{\varepsilon}(\boldsymbol{u})\right]^{1/2},$$

where c is a constant, usually taken as $c = 0.01$, the colon stands for the double contraction of second order tensors and h is the length of the element of the finite element discretization described later where the turbulent kinematic viscosity is to be computed. The total viscosity will be $\nu = \nu_{\rm mol} + \nu_{\rm tur}$, $\nu_{\rm mol}$ being the molecular viscosity.

Concerning the turbulent thermal diffusivity, it is taken of the form

$$\kappa_{\rm tur} = {\rm Pr}_{\rm tur}\nu_{\rm tur}, \tag{4}$$

where ${\rm Pr}_{\rm tur}$ is the turbulent Prandtl number, taken as ${\rm Pr}_{\rm tur} = 1$ in the numerical example. The total thermal diffusivity will be $\kappa = \kappa_{\rm mol} + \kappa_{\rm tur}$, $\kappa_{\rm mol}$ being the molecular thermal diffusivity.

In order to write the boundary conditions for equations (1)-(3), consider the boundary $\Gamma = \partial\Omega$ split into sets of disjoint components as $\Gamma = \overline{\Gamma_{\rm dv}\cup\Gamma_{\rm nv}\cup\Gamma_{\rm mv}}$ and also as $\Gamma = \overline{\Gamma_{\rm dt}\cup\Gamma_{\rm nt}}$, where $\Gamma_{\rm dv}$ and $\Gamma_{\rm dt}$ are the parts of the boundary with Dirichlet type boundary conditions for the velocity and the temperature, respectively, and $\Gamma_{\rm nv}$ and $\Gamma_{\rm nt}$ are those where Neumann type conditions are prescribed.

Mixed boundary conditions for the velocity are fixed on $\Gamma_{\rm mv}$. If the Cauchy stress tensor (divided by the density) is written as $\boldsymbol{\sigma} = -p\boldsymbol{I} + 2\nu\boldsymbol{\varepsilon}(\boldsymbol{u})$, the exterior normal to $\partial\Omega$ is $\boldsymbol{n}$, and prescribed values are represented by an overbar, the boundary conditions to be considered are

$$\boldsymbol{u}(\boldsymbol{x},t) = \bar{\boldsymbol{u}}(\boldsymbol{x},t) \quad \text{on } \Gamma_{\rm dv}, \tag{5}$$

$$\boldsymbol{n}\cdot\boldsymbol{\sigma}(\boldsymbol{x},t) = \boldsymbol{0} \quad \text{on } \Gamma_{\rm nv}, \tag{6}$$

$$\boldsymbol{n}\cdot\boldsymbol{u}(\boldsymbol{x},t) = 0 \text{ and } \boldsymbol{n}\cdot\boldsymbol{\sigma}(\boldsymbol{x},t)|_{\rm tang} = \bar{\boldsymbol{t}} \quad \text{on } \Gamma_{\rm mv}, \tag{7}$$

$$\vartheta(\boldsymbol{x},t) = \bar{\vartheta}(\boldsymbol{x},t) \quad \text{on } \Gamma_{\rm dt}, \tag{8}$$

$$\kappa\,\boldsymbol{n}\cdot\nabla\vartheta(\boldsymbol{x},t) = 0 \quad \text{on } \Gamma_{\rm nt}, \tag{9}$$

for $t \in (0, t_{\rm fin})$. In (7), $\boldsymbol{n}\cdot\boldsymbol{\sigma}(\boldsymbol{x},t)|_{\rm tang}$ denotes the component of the stress vector $\boldsymbol{n}\cdot\boldsymbol{\sigma}(\boldsymbol{x},t)$ tangent to $\partial\Omega$ and $\bar{\boldsymbol{t}}$ is the stress resulting from the standard wall law (see for example [20])

$$\bar{\boldsymbol{t}} = -\rho_0 \frac{U_*^2}{|\boldsymbol{u}|}\boldsymbol{u},$$

where U_* is the solution of the nonlinear equation

$$\frac{|\boldsymbol{u}|}{U_*} = \frac{1}{K}\log\left(\frac{U_*\Delta}{\nu}\right) + C,$$

with $K = 0.41$ (von Kármán constant), $C = 5.5$ and where Δ is the distance from the wall at which the velocity is evaluated.

To close the problem, initial conditions have to be appended to equations (1)-(3) and the boundary conditions (5)-(9). They are of the form $\boldsymbol{u}(\boldsymbol{x},0) = \boldsymbol{u}^0(\boldsymbol{x})$, $\vartheta(\boldsymbol{x},0) = \vartheta^0(\boldsymbol{x})$ for $\boldsymbol{x} \in \Omega$, where $\boldsymbol{u}^0(\boldsymbol{x})$ is a given initial velocity and $\vartheta^0(\boldsymbol{x})$ a given initial temperature.

In the numerical simulations of the telescope building, $\Gamma_{\rm dv}$ corresponds to the inflow part of the boundary of the computational domain, where the wind velocity is prescribed to a certain value of interest and with a given direction, whereas $\Gamma_{\rm nv}$ is the outflow boundary. The surface $\Gamma_{\rm mv}$ corresponds to both the ground surface and the building surface.

2.2 Finite element approximation

In order to discretize in space problem (1)-(3), let $\{\Omega^e\}$ be a finite element partition of the domain Ω, with index e ranging from 1 to the number of elements $n_{\rm el}$. We denote with a subscript h the finite element approximation to the unknown functions, and by $\boldsymbol{v}_h$, q_h and ψ_h the velocity, pressure and temperature test functions associated to $\{\Omega^e\}$, respectively.

A very important point is that we are interested in *using equal interpolation for all the unknowns* (velocity, pressure and temperature). Therefore, all the finite element spaces are assumed to be built up using the standard continuous interpolation functions. In particular, all the numerical simulations have been carried out using meshes of linear tetrahedra.

In order to overcome the numerical problems of the standard Galerkin method, a stabilized finite element formulation is applied. This formulation is presented in [6]. It is based on the subgrid scale concept introduced in [15], although when linear elements are used it reduces to the Galerkin/least-squares method described for example in [11] (see also [25]). We apply this stabilized formulation together with a finite difference approximation in time. The bottom line of the method is to test the continuous equations by the standard Galerkin test functions plus perturbations that depend on the operator representing the differential equation being solved. In our case, this operator corresponds to

the linearized form of the Navier-Stokes equations (1)-(2) and the heat equation (3). In this case, the method consists of finding $\boldsymbol{u}_h$, p_h and ϑ_h such that

$$\begin{aligned}
&\int_\Omega \boldsymbol{v}_h \cdot \boldsymbol{r}_{u1}\,\mathrm{d}\boldsymbol{x} + \int_\Omega 2\boldsymbol{\varepsilon}(\boldsymbol{v}_h) : \nu\boldsymbol{\varepsilon}(\boldsymbol{u}_h)\,\mathrm{d}\boldsymbol{x} - \int_\Omega p_h \nabla\cdot\boldsymbol{v}_h\,\mathrm{d}\boldsymbol{x} \\
&\quad + \sum_{e=1}^{n_{\mathrm{el}}} \int_{\Omega^e} \boldsymbol{\zeta}_{u1}\cdot(\boldsymbol{r}_{u1}+\boldsymbol{r}_{u2})\,\mathrm{d}\boldsymbol{x} + \sum_{e=1}^{n_{\mathrm{el}}} \int_{\Omega^e} \zeta_{u2}\, r_p\,\mathrm{d}\boldsymbol{x} \\
&\quad = \sum_{e=1}^{n_{\mathrm{el}}} \int_{\Omega^e} (\boldsymbol{v}_h + \boldsymbol{\zeta}_{u1})\cdot\boldsymbol{f}\,\mathrm{d}\boldsymbol{x} + \int_{\Gamma_{\mathrm{mv}}} \boldsymbol{v}_h\cdot\bar{\boldsymbol{t}}\,\mathrm{d}\Gamma, \\
&\int_\Omega q_h r_p\,\mathrm{d}\boldsymbol{x} + \sum_{e=1}^{n_{\mathrm{el}}} \int_{\Omega^e} \boldsymbol{\zeta}_p\cdot(\boldsymbol{r}_{u1}+\boldsymbol{r}_{u2})\,\mathrm{d}\boldsymbol{x} = \sum_{e=1}^{n_{\mathrm{el}}} \int_{\Omega^e} \boldsymbol{\zeta}_p\cdot\boldsymbol{f}\,\mathrm{d}\boldsymbol{x}, \\
&\int_\Omega \psi_h\cdot r_{\vartheta 1}\,\mathrm{d}\boldsymbol{x} + \int_\Omega \kappa\nabla\psi_h\cdot\nabla\vartheta_h\,\mathrm{d}\boldsymbol{x} + \sum_{e=1}^{n_{\mathrm{el}}} \int_{\Omega^e} \zeta_\vartheta\,(r_{\vartheta 1}+r_{\vartheta 2})\,\mathrm{d}\boldsymbol{x} = 0,
\end{aligned}$$

for all test functions $\boldsymbol{v}_h$, q_h and ψ_h, where

$$\boldsymbol{r}_{u1} := \partial_t\boldsymbol{u}_h + \boldsymbol{g}\beta\vartheta_h + (\boldsymbol{u}_h\cdot\nabla)\boldsymbol{u}_h, \tag{10}$$
$$\boldsymbol{r}_{u2} := -2\nabla\cdot[\nu\boldsymbol{\varepsilon}(\boldsymbol{u}_h)] + \nabla p_h, \tag{11}$$
$$r_p := \nabla\cdot\boldsymbol{u}_h, \tag{12}$$
$$r_{\vartheta 1} := \partial_t\vartheta_h + (\boldsymbol{u}_h\cdot\nabla)\vartheta_h, \tag{13}$$
$$r_{\vartheta 2} := -\nabla\cdot(\kappa\nabla\vartheta_h), \tag{14}$$

the functions $\boldsymbol{\zeta}_{u1}$, ζ_{u2} and $\boldsymbol{\zeta}_p$ are computed within each element as

$$\boldsymbol{\zeta}_{u1} = \tau_u\left\{(\boldsymbol{u}_h\cdot\nabla)\boldsymbol{v}_h + 2\nabla\cdot[\nu\boldsymbol{\varepsilon}(\boldsymbol{v}_h)]\right\}, \tag{15}$$
$$\zeta_{u2} = \tau_p\nabla\cdot\boldsymbol{v}_h, \tag{16}$$
$$\boldsymbol{\zeta}_p = \tau_u\nabla q_h, \tag{17}$$
$$\zeta_\vartheta = \tau_\vartheta\left[(\boldsymbol{u}_h\cdot\nabla)\psi_h + \nabla\cdot(\kappa\nabla\psi_h)\right], \tag{18}$$

and the parameters τ_u, τ_p and τ_ϑ are also computed element-wise as (see [6])

$$\begin{aligned}
\tau_u &= \left[\frac{4\nu}{h^2} + \frac{2|\boldsymbol{u}_h|}{h}\right]^{-1}, \\
\tau_p &= 4\nu + 2|\boldsymbol{u}_h|h, \\
\tau_\vartheta &= \left[\frac{4\kappa}{h^2} + \frac{2|\boldsymbol{u}_h|}{h}\right]^{-1},
\end{aligned}$$

where h is the element size for linear elements and half of it for quadratics.

From (15)-(18) it is observed that these terms are precisely the adjoints of the (linearized) operators of the differential equations to be solved applied to the test functions (observe the signs of the viscous term in (15) and of the diffusive term in (18)). This method corresponds to the algebraic version of the subgrid scale approach ([15]) and circumvents *all* the stability problems of the Galerkin method. In particular, in this case it is possible to use equal velocity pressure interpolations, that is, we are not tight to the satisfaction of the inf-sup stability condition.

A controversial issue is whether the stabilized formulation presented is able to act as a turbulence model, that is to say, if the Smagorinsky viscosity can be turned off. This possibility is advocated in [8, 2]. Even though our numerical simulations have been performed using the Smagorinsky model, some runs without it have provided good results with richer dynamics.

2.3 Some implementation issues

Apart from a more or less standard iterative procedure to deal with the different nonlinearities, the basic numerical formulation presented above has been implemented using some features which will not be detailed here. These are:

- Time integration can be performed with any finite difference scheme. In particular, the example of Section 4 has been simulated using the second order Crank-Nicolson method.
- Nodal based implementation [5]. This implementation is based on an a priori calculation of the integrals appearing in the formulation and then the construction of the matrix and right-hand-side vector of the final algebraic system to be solved. After appropriate approximations, this matrix and this vector can be constructed directly for each nodal point, without the need to loop over the elements and thus making the calculations much faster. In order to be able to do this, all the variables have to be defined at the nodes of the finite element mesh, not on the elements. This is also so for the stabilization parameters of the formulation.
- Block-iterative coupling to segregate the velocity-pressure and temperature calculations [4]. A single iterative loop is used to deal both with the nonlinearities of the problem and with the temperature coupling with the Navier-Stokes equations.
- Predictor corrector scheme [7]. The pressure segregation is inspired in fractional step schemes, although the converged solution corresponds to that of a monolithic time integration.

The reader is referred to the references indicated in each item for details.

3 Optical parameters

In this section we introduce the parameters that allow us to measure the quality of the seeing of a site, and we also describe their numerical approximation in the context of the finite element formulation for the flow equations presented above.

3.1 Physical background

The optical parameters we are interested in are the Fried parameter and the Greenwood frequency. In fact, they are both obtained from integration of a function of the structure constant of the refractive index along an optical path. Let us start describing the problem and leave for the next subsection its approximation (see [22] for more details).

Let $n(\boldsymbol{x}, t)$ be the refractive index of a medium. Optical quality depends on spatial and temporal variability of this parameter, basically due to temperature and humidity fluctuations. In particular, we are interested in the structure function of n, defined as

$$D_n(\boldsymbol{x}, \boldsymbol{x}') = \langle [n(\boldsymbol{x}, t) - n(\boldsymbol{x}', t)]^2 \rangle. \tag{19}$$

Here, $\langle \cdot \rangle$ denotes the ensemble average. However, under the ergodicity assumption we will replace it, in (19) and below, by the time average over a time window of period T, large enough to make $D_n(\boldsymbol{x}, \boldsymbol{x}')$ (almost) time independent. Likewise, we will assume isotropic turbulence, so that D_n depends only on $r := |\boldsymbol{x} - \boldsymbol{x}'|$, not on $\boldsymbol{x}'$. This dependence will be written as $D_n(\boldsymbol{x}, r)$. Moreover, if we assume further

that $1/r$ belongs to the inertial range of the Kolmogorov spectrum, it can be shown by dimensional analysis that (see [24])

$$D_n(\boldsymbol{x}, r) = C_n^2(\boldsymbol{x}) r^{2/3}, \tag{20}$$

where $C_n(\boldsymbol{x})$ is the constant of structure of n. See also [26] for a discussion about the limits of this approximation.

Given a point $\boldsymbol{x} \in \Omega$, let us consider a beam of light arriving to $\boldsymbol{x}$ with the direction given by a unit vector $\boldsymbol{l}$. To integrate along this beam of light, we may consider it *starting from* rather than *arriving to* $\boldsymbol{x}$, and parametrize it as $\boldsymbol{x} + s\boldsymbol{l}$, with $s \in [0, \infty)$. Having introduced this notation, the optical path length δ_l and the phase fluctuation φ_l can be computed as

$$\delta_l(\boldsymbol{x}, t) = \int_0^\infty n(\boldsymbol{x} + s\boldsymbol{l}, t) \mathrm{d}s, \quad \varphi_l(\boldsymbol{x}, t) = \frac{2\pi}{\lambda} \int_0^\infty n(\boldsymbol{x} + s\boldsymbol{l}, t) \mathrm{d}s, \tag{21}$$

where λ is the wavelength of the wavefront of the light beam. Note that subscript l refers to the direction of the light beam.

To obtain the variability of φ_l (and therefore the relative change in the wave phase) its structure function is needed. It is given by

$$D_{\varphi_l}(\boldsymbol{x}, \xi) = \langle [\varphi_l(\boldsymbol{x}, t) - \varphi_l(\boldsymbol{x} + \boldsymbol{\xi}, t)]^2 \rangle,$$

where $\xi = |\boldsymbol{\xi}|$. Making use of (21) and (20) it can be shown that (see [22])

$$D_{\varphi_l}(\boldsymbol{x}, \xi) = 2.91 \left(\frac{2\pi}{\lambda} \right)^2 \xi^{5/3} \int_0^\infty C_n^2(\boldsymbol{x} + s\boldsymbol{l}) \mathrm{d}s.$$

This expression can be written in terms of the *Fried parameter* r_0 as

$$D_{\varphi_l}(\boldsymbol{x}, \xi) = 6.88 \left(\frac{\xi}{r_0} \right)^{5/3},$$

where

$$r_0 = r_0(\boldsymbol{l}; \boldsymbol{x}) = \left(\frac{16.6}{\lambda^2} \int_0^\infty C_n^2(\boldsymbol{x} + s\boldsymbol{l}) \mathrm{d}s \right)^{-3/5}. \tag{22}$$

Note that once again we have made explicit the dependence of r_0 on the spatial point and the light beam direction. Obviously, it also depends on the wavelength of the light wave, λ.

The importance of r_0 is due to the fact the mean-square distortion of a wavefront over a circle of area A and diameter d centered at a point $\boldsymbol{x}$, normal to $\boldsymbol{l}$, parametrized by $\boldsymbol{x} + \boldsymbol{y}$ and given by

$$\sigma_1^2 = \sigma_1^2(\boldsymbol{l}; \boldsymbol{x}) = \frac{4}{\pi d^2} \int_A \langle [\varphi_l(\boldsymbol{x} + \boldsymbol{y}, t) - \varphi_{0,l}(\boldsymbol{x}, t)]^2 \rangle \mathrm{d}\boldsymbol{y},$$
$$\varphi_{0,l}(\boldsymbol{x}, t) := \frac{4}{\pi d^2} \int_A \varphi_l(\boldsymbol{x} + \boldsymbol{y}, t) \mathrm{d}\boldsymbol{y},$$

can be shown to be (see [22])

$$\sigma_1^2 = 1.03 \left(\frac{d}{r_0} \right)^{5/3}.$$

Thus, if $d = r_0$ the root-mean-square (RMS) distortion is approximately 1 radian.

The Fried parameter r_0 is essential in adaptive optics. In the case of telescopes it allows to determine the number of segments into which a segmented mirror has to be split, or the distance between actuators for a continuous deformable mirror, by prescribing an admissible RMS distortion of a wavefront [3]. But the design of their actuators is also based on the so called *Greenwood frequency*, which is an indication of how fast the atmosphere is changing and defines the bandwidth of the servo control for an adaptive optics system. This frequency is defined as

$$f_G = 0.43 \frac{V_{\text{wind}}}{r_0} \tag{23}$$

where V_{wind} is a weighted mean wind velocity defined as

$$V_{\text{wind}} = V_{\text{wind}}(\boldsymbol{l}; \boldsymbol{x}) = \left(\frac{\int_0^\infty \langle |\boldsymbol{u}| \rangle^{5/3} C_n^2(\boldsymbol{x} + s\boldsymbol{l}) \mathrm{d}s}{\int_0^\infty C_n^2(\boldsymbol{x} + s\boldsymbol{l}) \mathrm{d}s} \right)^{3/5}. \tag{24}$$

The problem of computing r_0 and f_G is reduced to the problem of computing the structure function of the refractive index, C_n, and then computing the integrals in (22) and (24). In turn, this structure function can be related to the structure function of the temperature, the humidity and their joint structure parameter (see [19]). However, we will consider the humidity effects negligible. Thus, if we write the temperature dependence of n as $n = n(\vartheta)$, we have

$$C_n = \frac{\mathrm{d}n}{\mathrm{d}\vartheta} C_\vartheta,$$

where C_ϑ is the structure function of the temperature. Assuming pressure equilibrium it is found that [24]

$$C_n = \frac{79 \times 10^{-6}}{\langle \vartheta \rangle^2} \langle p \rangle C_\vartheta, \tag{25}$$

where p is assumed to be measured in millibars and ϑ is the absolute temperature. Here and below, ϑ, p and $\boldsymbol{u}$ denote the solution of the continuous problem *without* using a LES model, that is to say, with $\nu_{\text{tur}} = 0$, $\kappa_{\text{tur}} = 0$ in (1)-(3).

In view of (25), the problem is to compute C_ϑ. Once again in the inertial range of the Kolmogorov spectrum and assuming the temperature to be a passive quantity, it can be shown that (see [22])

$$C_\vartheta^2 = a^2 \chi \varepsilon^{-1/3}, \tag{26}$$

where a is an empirical value called Obukhov-Corrsin constant (see [14, 27] for extensions and a discussion about Obukhov-Corrsin constants and on the validity of this approximation). In (26), χ denotes the mean thermal diffusive dissipation and ε the mean dissipation of kinetic energy of the flow. These parameters are given by

$$\chi := \kappa_{\text{mol}} \langle |\nabla \vartheta|^2 \rangle, \quad \varepsilon := \nu_{\text{mol}} \langle |\boldsymbol{\varepsilon}(\boldsymbol{u})|^2 \rangle. \tag{27}$$

The problem is now closed: using (27) in (26) and the result back in (25) we have an expression to compute C_n in terms of the flow variables $\boldsymbol{u}$, p, ϑ at each point.

The question now is how to apply this development in the context of a LES simulation and, more precisely, using the flow variables $\boldsymbol{u}_h$, p_h, ϑ_h resulting from the finite element approximation of a LES model as described in the previous section. The first point to consider is that filtered unknowns

appearing in a LES model need to maintain the mean of the original variables. *Assuming* this to hold also for their finite element approximation we have that

$$\langle \boldsymbol{u} \rangle \approx \langle \boldsymbol{u}_h \rangle, \quad \langle p \rangle \approx \langle p_h \rangle, \quad \langle \vartheta \rangle \approx \langle \vartheta_h \rangle. \tag{28}$$

The second point is that the dissipation of the continuous problem is approximately equal to the dissipation of the LES approximation using the effective turbulent thermal diffusion, in the case of the heat dissipation, or effective turbulent kinematic viscosity, in the case of the mechanical dissipation. This is in fact the main requirement posed by Lilly to LES models [17, 20], and the key feature for their design [9]. Moreover, it is also shown in [13] that the numerical formulation presented in Section 2 *introduces also a mechanical numerical dissipation proportional to the viscous dissipation*. This leads us to assume that

$$\kappa_{\rm mol} \langle |\nabla \vartheta|^2 \rangle \approx \kappa_{\rm tur} \langle |\nabla \vartheta_h|^2 \rangle, \quad \nu_{\rm mol} \langle |\boldsymbol{\varepsilon}(\boldsymbol{u})|^2 \rangle \approx \nu_{\rm tur} \langle |\boldsymbol{\varepsilon}(\boldsymbol{u}_h)|^2 \rangle. \tag{29}$$

Using approximations (28) and (29) in (26) and inserting the result in (25) it is found that

$$C_n = 79 \times 10^{-6} \langle \vartheta_h \rangle^{-2} \, \langle p_h \rangle \, a \, \nu_{\rm tur}^{1/3} \langle |\nabla \vartheta_h|^2 \rangle^{1/2} \langle |\boldsymbol{\varepsilon}(\boldsymbol{u}_h)|^2 \rangle^{-1/6}, \tag{30}$$

where we have assumed that $\mathrm{Pr}_{\rm tur} = 1$ in (4). Equation (30) is the expression we were looking for. It allows us to compute the structure function of the refractive index in terms of the flow variables resulting from a LES numerical simulation. Using this expression in (22) and in (24), also replacing $\boldsymbol{u}$ by $\boldsymbol{u}_h$ in this last case, the Fried parameter and the Greenwood frequency can be computed. We present next the algorithm to compute the integrals in (22) and (24).

3.2 Numerical strategy

Expression (30) allows us to compute the structure constant of the refractive index at each node of the finite element mesh introduced in Section 2 to approximate the flow equations. The only remark is that the derivatives of $\boldsymbol{u}_h$ appearing in $\boldsymbol{\varepsilon}(\boldsymbol{u}_h)$ and the derivatives of ϑ_h appearing in $\nabla \vartheta_h$ will be discontinuous, usually computed at the numerical integration points. They can be approximated by continuous functions by using a classical L^2 projection. To simplify the exposition, we will assume that this approximation is done, although it is not necessary (and in fact we have not used it in the numerical example).

Equations (22) and (24), with the continuous functions approximated by finite element functions defined at the nodes of the finite element mesh, imply an integral along the light beam. Therefore, our concern now is to compute integrals of the form

$$I(\boldsymbol{l}; \boldsymbol{x}) = \int_0^\infty F_h(\boldsymbol{x} + s\boldsymbol{l}) \mathrm{d}s, \tag{31}$$

where the finite element function $F_h(\boldsymbol{x})$ is an approximation to C_n^2 in the case of (22) and the denominator in (24) and an approximation to $\langle |\boldsymbol{u}| \rangle^{5/3} C_n^2$ in the case of the numerator in (24). Note that F_h would be discontinuous across interelement boundaries if $\boldsymbol{\varepsilon}(\boldsymbol{u}_h)$ and $\nabla \vartheta_h$ are not approximated by continuous functions.

First of all, it is obvious that the computational domain is finite. For simplicity, let us assume that the upper boundary of Ω is the plane $z = Z$, z being the vertical coordinate. Let $S = S(\boldsymbol{l}; \boldsymbol{x})$ be the distance from a point $\boldsymbol{x}$ to $\partial\Omega$ in the direction of vector $\boldsymbol{l}$ and let also γ be the angle between $\boldsymbol{l}$ and the vertical axes, so that $s = s(z) = \sec\gamma(z - Z) + S$ (see Figure 1).

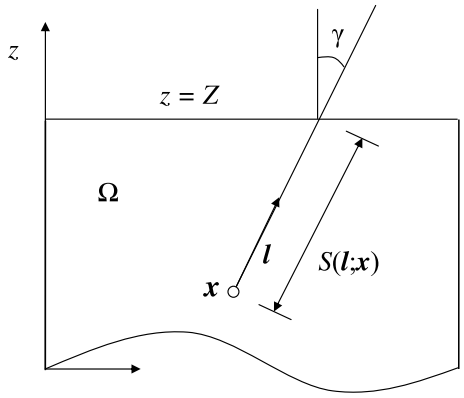

Figure 1: Notation for the integrals in (32)

Considering only points $\boldsymbol{x} \in \Omega$ such that the light beam crosses the plane $z = Z$, we may split the integral in (31) as

$$I(\boldsymbol{l};\boldsymbol{x}) = \int_0^S F_h(\boldsymbol{x} + s\boldsymbol{l})\mathrm{d}s + \sec\gamma \int_Z^\infty F_h(\boldsymbol{x} + s(z)\boldsymbol{l})\mathrm{d}z. \tag{32}$$

The first term in the right-hand-side of this expression is what needs to be computed numerically. The second term is considered to be known from empirical data. In fact, in the case $F_h(\boldsymbol{x}) \approx \langle|\boldsymbol{u}|\rangle^{5/3}C_n^2$ it is assumed that the mean velocity is constant for $z > Z$, so that what is needed is only $\int_Z^\infty C_n^2\mathrm{d}z$. Values for this number can be found for example in [21].

Let us explain how to compute the first integral in (32). We assume in the description of the following algorithm that the elements used are linear tetrahedra. The steps to be performed are the following:

- (Pre-process) Determine the element domains $\{e_1, ..., e_{n_{\mathrm{beam}}}\} \in \{1, 2, ..., n_{\mathrm{el}}\}$ crossed by the light beam:
  - ▷ Given a point $\boldsymbol{x} \in \Omega$ determine the element e_1 to which it belongs. This can be done by looping over the elements and checking for which element the natural coordinates of $\boldsymbol{x}$ belong to the parent domain (see [18], for example). See Figure 2.
  - ▷ Find the intersection $\boldsymbol{y}$ of the line passing by $\boldsymbol{x}$ with direction $\boldsymbol{l}$ with the boundary of element e_1.
  - ▷ Determine the element e_2 to which point $\boldsymbol{y}$ belongs.
  - ▷ Find the intersection $\boldsymbol{y}'$ of the line passing by $\boldsymbol{y}$ with direction $\boldsymbol{l}$ with the boundary of element e_2.
  - ▷ Proceed until exiting the computational domain. We denote $\boldsymbol{y}_i$, $\boldsymbol{y}_i'$ the points obtained following this process in element e_i, $i = 2, ..., n_{\mathrm{beam}}$.
- (Pre-process) Locate the arc coordinates $s_{e_i,j}$ for $j = 1, ..., n_{\mathrm{int}}$ within each e_i, $i = 1, ..., n_{\mathrm{beam}}$, of the integration points and determine the weights $w_{e_i,j}$ of the numerical integration rule:

$$\int_0^S F_h(\boldsymbol{x} + s\boldsymbol{l})\mathrm{d}s \approx \sum_{i=1}^{n_{\mathrm{beam}}}\sum_{j=1}^{n_{\mathrm{int}}} w_{e_i,j}F_h(\boldsymbol{x} + s_{e_i,j}\boldsymbol{l}). \tag{33}$$

  Any numerical integration rule can be used. The arc coordinates can be found transforming the integration path $\boldsymbol{y}_i' - \boldsymbol{y}_i$ (or $\boldsymbol{y}_1' - \boldsymbol{x}$ in the case of element e_1) within each element (see Figure 2)

to the reference interval of the particular integration rule. For example, for the Gauss-Legendre rule used in the numerical simulation of the following section, if $s_{e_i,0}$ is the arc coordinate of point $\boldsymbol{y}_i$ for element e_i,

$$s_{e_i,j} = s_{e_i,0} + \frac{1}{2}(1+\eta_j)|\boldsymbol{y}_i' - \boldsymbol{y}_i|, \quad w_{e_i,j} = \frac{1}{2}|\boldsymbol{y}_i' - \boldsymbol{y}_i|\omega_j, \quad j = 1, ..., n_{\text{int}},$$

where η_j and ω_j are the coordinates and weights of the j-th integration point in the interval $[-1, 1]$.

- (Post-process) Once the LES simulation has finished, obtain the nodal values of the time averaged flow variables and, from them, the nodal values of $F_h(\boldsymbol{x})$ (if derivatives are not approximated by continuous functions, F_h will be discontinuous).
- (Post-process) Interpolate from the nodes of each element to the numerical integration points and perform the numerical integral (33).

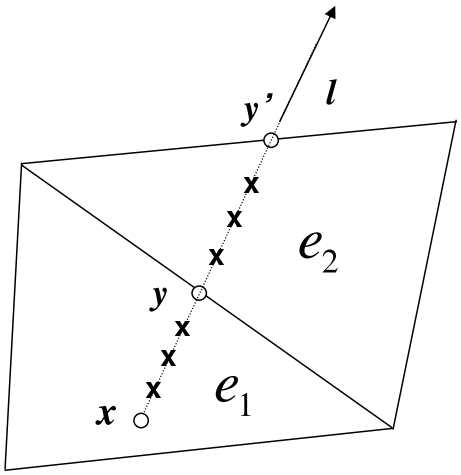

Figure 2: Line integration within an element. The crosses denote the numerical integration points.

4 An example of application

In this section we present an application of the numerical strategy described in the previous sections to the calculation of the Fried parameter and Greenwood frequency around a telescope. The example to be shown corresponds to the project of a solar telescope, the Advanced Technology Solar Telescope (ATST) [1], in which study the Astrophysical Institute of the Canary Islands has been involved. The results to be presented do not correspond to a real situation, but to a preliminary analysis to determine the convenience of the project. Their purpose is not an exact quantitative analysis of the problem, but a qualitative demonstration of the possibilities of the formulation proposed herein.

The physical properties used in the numerical approximation of (1)-(3) are those of air at normal conditions.

The site to be analyzed is located in the observatory of *El Roque de los Muchachos*, in the La Palma island of the Canary archipelago. Figure 3 shows a general view of the site with the surface finite element mesh used to discretize what we will call the *large* computational domain. This domain is used for a preliminary simulation used to determine the boundary conditions of a more detailed calculation.

The region of the island analyzed has 10×7.6 km^2 and a height of 1400 m above the sea level. A semisphere of radius 14.2 km is the computational domain (see Figure 3). The mesh used has only 9.2×10^4 linear tetrahedral elements. Steady-state calculations (understood as a Reynolds averaged Navier-Stokes simulations) have been performed with different wind directions and wind intensities, considered representative of the site. In the following, only results corresponding to a uniform wind of 4 m/s coming from the west will be considered. In upper atmospheric layers, this wind is not perturbed, while near the ground its direction and speed are altered by the terrain geometry and buildings. The velocity of 4 m/s is imposed as boundary condition at the inflow nodes of the spherical computational domain mentioned.

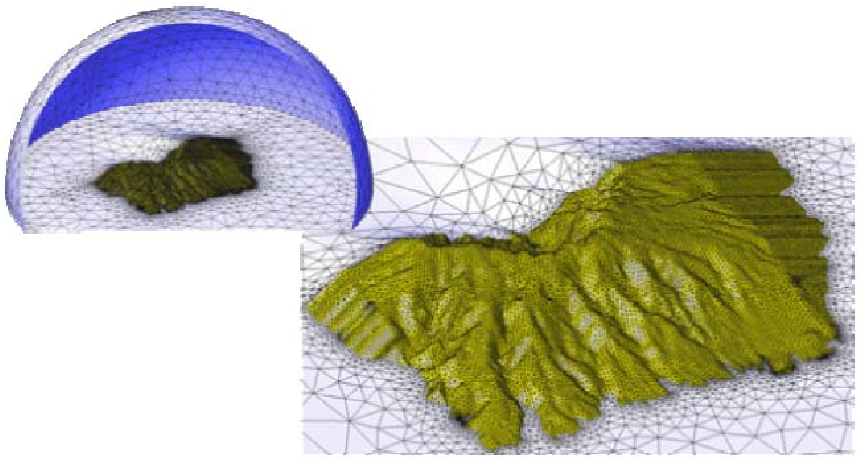

Figure 3: General view and detail of the large scale computational domain

Results obtained for the large computational region are used as boundary conditions for the small scale domain where the simulations will be actually carried out, now introducing the ATST telescope as well as the other existing buildings hosting telescopes. Only results for one of the sites analyzed will be shown. The extension of the small computational domain has 1217000 m^2 and it is discretized using a mesh of 3.2×10^6 linear tetrahedral elements (see Figure 4). It corresponds to a sphere of diameter 28450 m, the minimum distance from the telescope to the boundary being 12500 m.

As it has been mentioned, velocity boundary conditions for the small scale domain are obtained from the large scale domain. Standard interpolation between meshes is used. Concerning the temperature, we have assumed a near ground temperature profile in the vertical coordinate z of the form

$$T = T_0 - T_{\rm dec} \frac{\log z - \log z_h}{\log H - \log z_h}, \quad z \geq z_h. \tag{34}$$

We have taken the rugosity parameter $z_h = 0.02$ m, the temperature at $z = z_h$ as $T_0 = 12$ °C, and the temperature decrease $T_{\rm dec} = 4$ °C for $H = 6$ m. See [16] for a motivation and discussion about this type of logarithmic laws. When the slope $\partial T/\partial z$ of the curve given by (34) is -0.0065 we replace it by a linear law that yields a decrease of 6.5 °C each km. Likewise, $T = T_0 = 12$ has been chosen for $0 \leq z \leq z_h$. These data correspond to the mean temperatures on the ground during winter and the measured temperature difference between 0 and 6 m (4 °C). The temperature distribution obtained is prescribed on the ground and at the upper boundary of the computational domain and it is used as initial condition for the nodes of the rest of the computational domain.

Results of the numerical simulation of the aerodynamic problem are shown in Figures 5 to 8. These results have been shown on two vertical plane sections, one along the middle of the telescope building

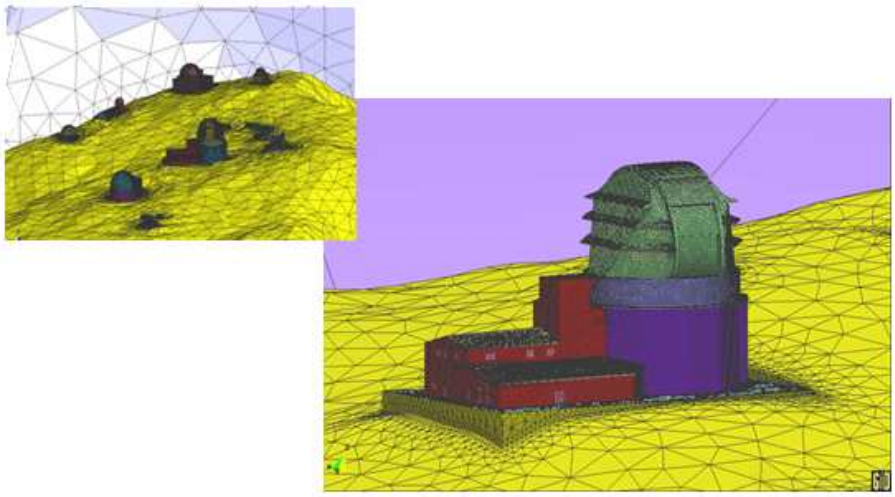

Figure 4: General view of the small scale computational domain and mesh around the ATST telescope

and crossing the auxiliary building (see Figure 4) and the other perpendicular to the former, also passing through the middle of the telescope building. It is worth noting that turbulence is formed around the building on the side opposite to the wind.

Once the flow variables have been computed, we may proceed to compute the distribution of the structure constant of the refractive index , C_n^2, using expression (30). Results are shown in Figure 9. It is known that typical values of C_n^2 are 10^{-14} $\mathrm{m}^{-2/3}$ close to the ground and 10^{-17} $\mathrm{m}^{-2/3}$ at 10 km height. This is the order of magnitude of the values we have computed, except for points very close to the surfaces, where high fluctuations of velocity and temperature lead to larger values of C_n^2.

The last step is to compute the Fried parameter r_0 and the Greenwood frequency f_G using the methodology explained in the previous Section. First, let us note that the pre-process steps in the algorithm described there yield a set of elements crossed by a light beam as the one shown in Figure 10.

The results obtained for different directions of the light beam (that is to say, different vectors $\boldsymbol{l}$) are given in Table 1. These directions are expressed in terms of the azimuth and the zenital angle from an observation point located at the middle of the telescope building and on the dome surface, close to where the main mirror of the telescope should be placed. Despite the position of the sun on the sky is restricted to the ecliptic and, consequently, a solar telescope like ATST will only observe in those directions, we present the results for all azimuthal angles for completeness.

The third column in Table 1 gives the first term in (32) when $F_h = C_n^2$, whereas the fourth gives the total integral, with the second contribution obtained from [21]. The Fried parameter for $\lambda = 500$ nm is given in the fifth column. It is known for example that typical values of r_0 (for $\lambda = 900$ nm) at good sites are of the order of 20–40 cm (during daylight, as in our case), so that our results have the correct order of magnitude. From tables similar to Table 1 computed from different heights (not from the dome surface) it can also be shown that r_0 decreases rapidly with height, as it should be expected.

The sixth and seventh columns are preliminary results to compute f_G, whose values are given in the last column. Again, the order of magnitude obtained is correct. Despite turbulence is mainly concentrated on the part of the building not facing the wind, the results show that there is no dependence of r_0 with the azimuthal angle. V_{wind}, however, is minimum in a direction parallel to the wind (azimuth values of 90° and 270°), leading to smaller Greenwood frequencies.

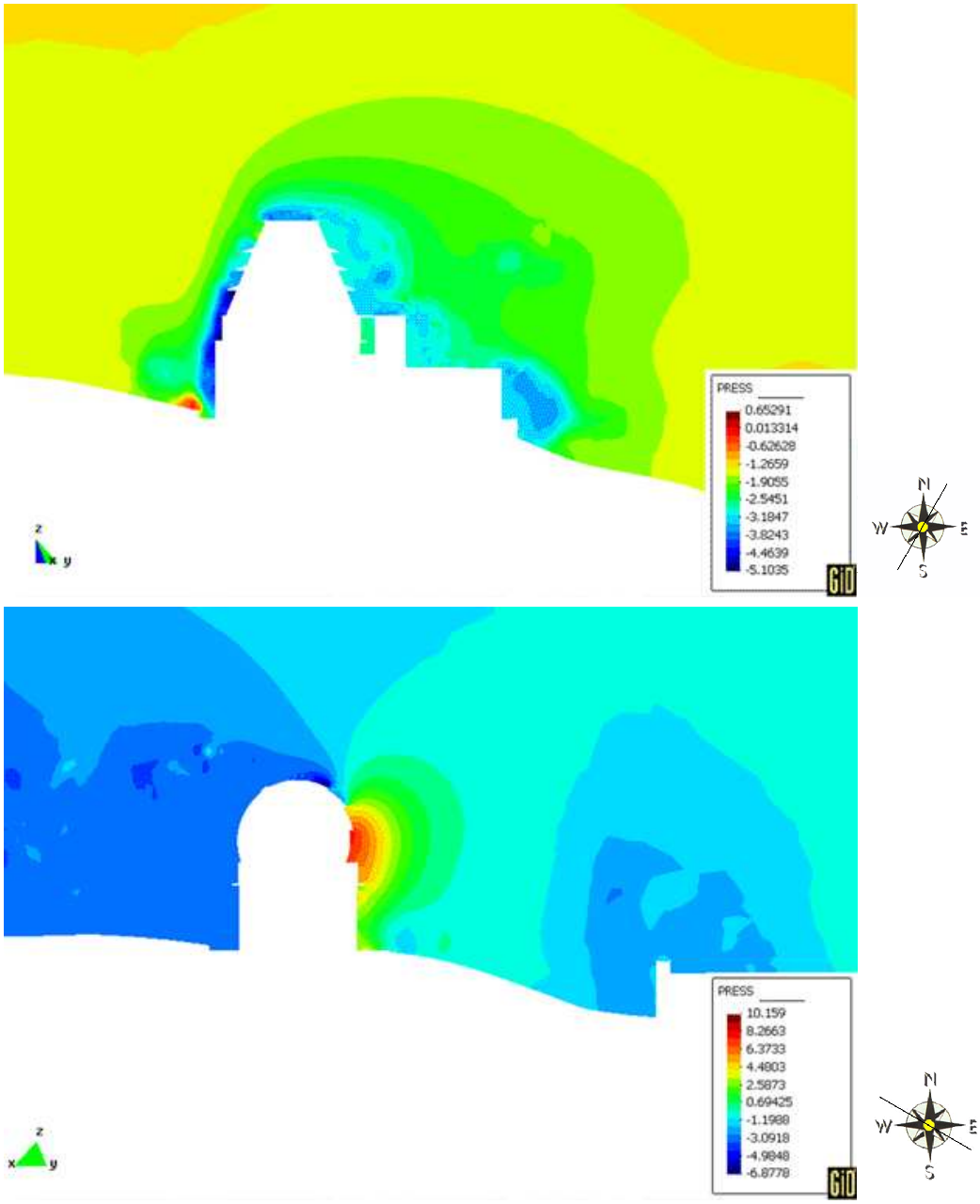

Figure 5: Mean pressure contours along a longitudinal and a transverse cut

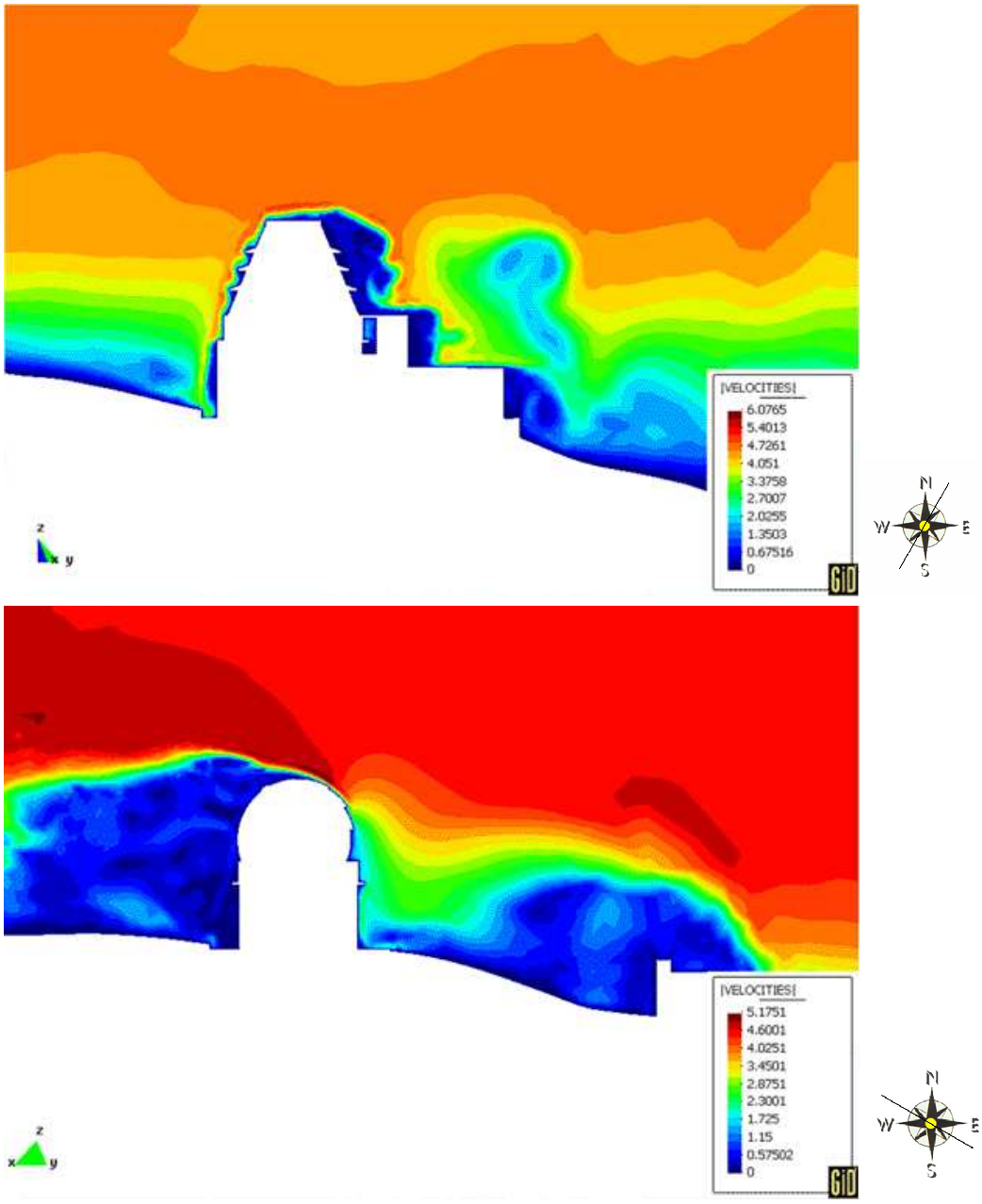

Figure 6: Contours of the norm of the mean velocity along a longitudinal and a transverse cut

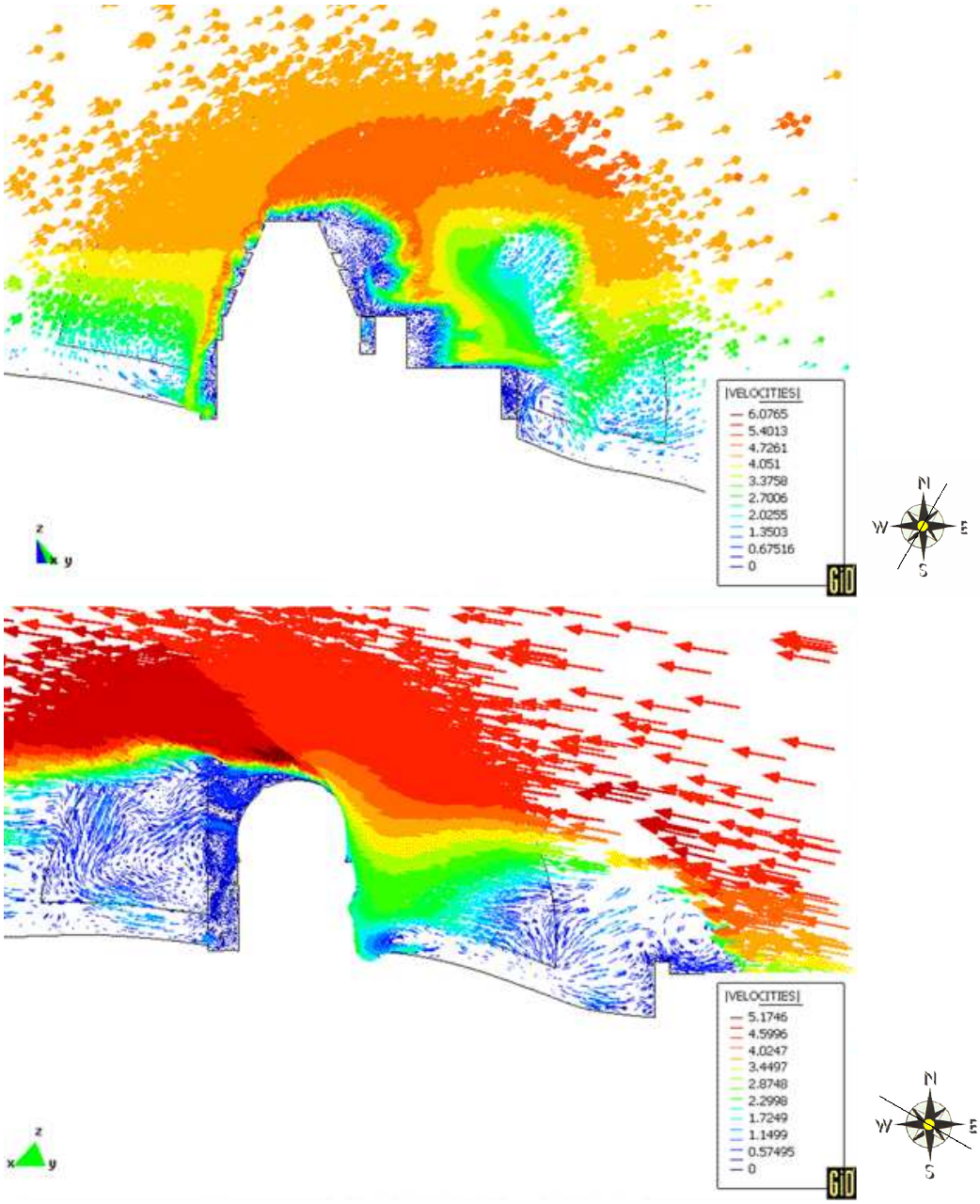

Figure 7: Mean velocity vectors along a longitudinal and a transverse cut

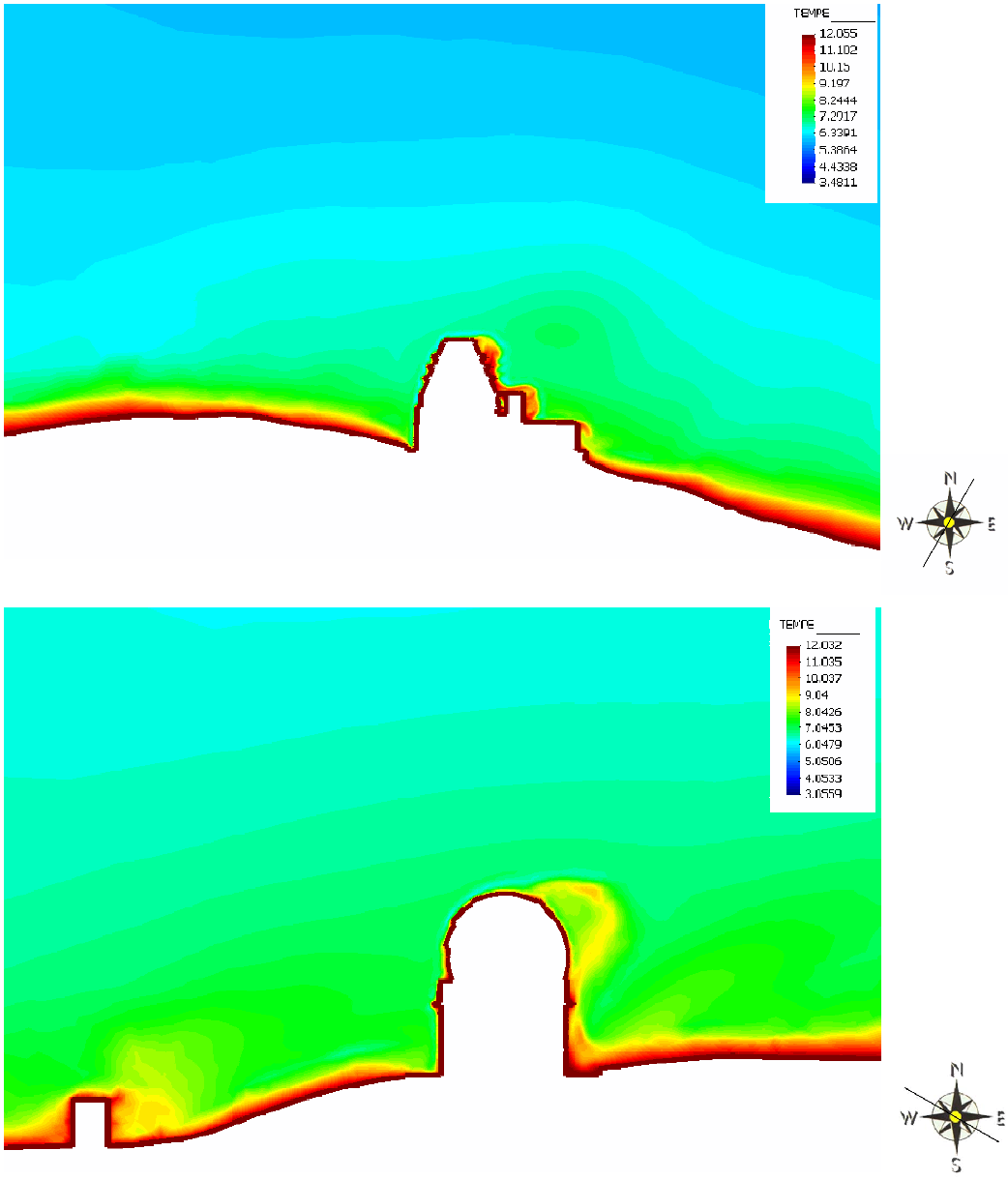

Figure 8: Mean temperature contours along a longitudinal and a transverse cut

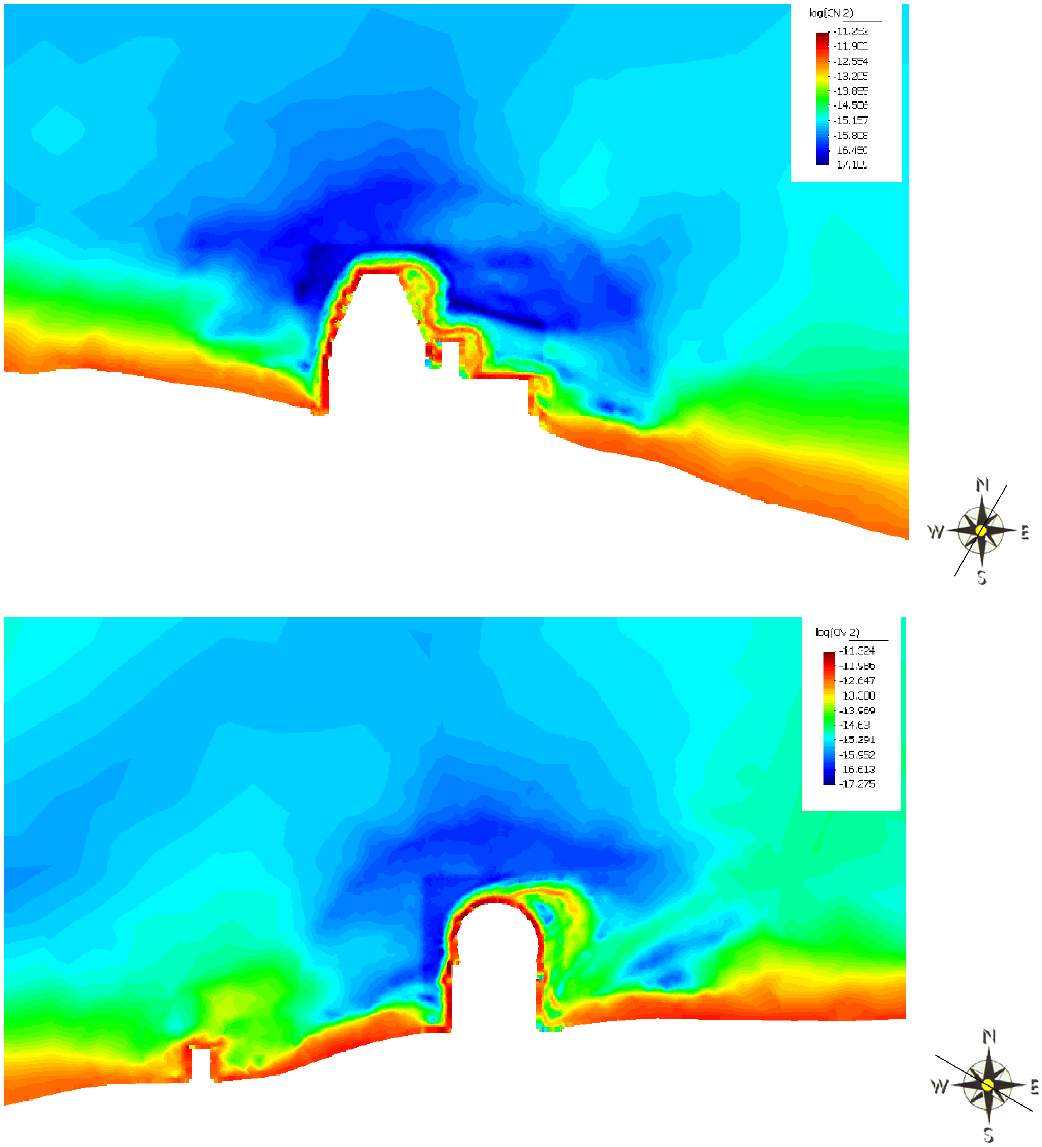

Figure 9: Contours of C_n^2 along a longitudinal and a transverse cut

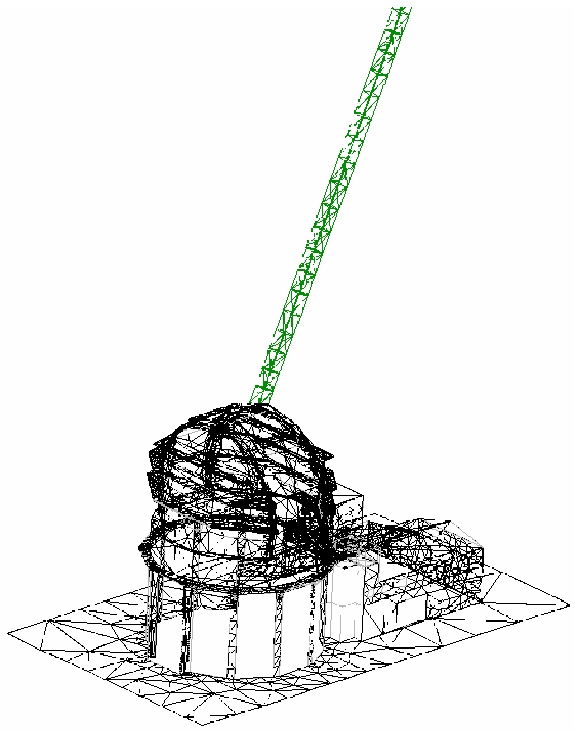

Figure 10: Elements crossed by a light beam

Azimuth	Zenital angle	$\int_0^S C_n^2 \mathrm{d}s$ $\times 10^{12}$	$\int_0^\infty C_n^2 \mathrm{d}s$ $\times 10^{12}$	r_0 (m)	$\int_0^S \langle \lvert \boldsymbol{u}_h \rvert^{5/3} \rangle C_n^2 \mathrm{d}s$ $\times 10^{11}$	V_{wind} (m/s)	f_G (Hz)
0°	0°	2.35	2.63	0.0452	1.47	3.01	28.63
0°	30°	3.58	3.90	0.0356	2.63	3.31	39.95
45°	30°	3.18	3.50	0.0381	1.96	2.98	33.70
90°	30°	2.60	2.93	0.0424	1.37	2.71	27.54
135°	30°	2.65	2.98	0.0419	1.86	3.22	33.03
180°	30°	3.32	3.65	0.0371	2.95	3.70	42.92
225°	30°	2.56	2.88	0.0427	1.06	2.35	23.62
270°	30°	2.68	3.01	0.0417	9.81	2.18	22.46
315°	30°	2.66	2.98	0.0419	1.19	2.45	25.18
0°	60°	5.31	5.87	0.0279	3.41	3.05	47.02
45°	60°	4.70	5.26	0.0298	2.34	2.62	37.84
90°	60°	5.19	5.75	0.0282	2.03	2.26	34.49
135°	60°	4.41	4.97	0.0308	2.07	2.53	35.30
180°	60°	5.59	6.15	0.0271	4.06	3.29	52.09
225°	60°	4.25	4.81	0.0314	1.81	2.39	32.65
270°	60°	4.82	5.38	0.0294	1.26	1.78	26.04
315°	60°	4.14	4.70	0.0319	6.99	1.37	18.47

Table 1: Results for the optical parameters. Azimuths are measured clockwise from the North.

5 Concluding remarks

The purpose of this paper has been to present a numerical formulation to compute the optical parameters in a turbulent flow. It has *not* been our intention to show quantitatively correct calculations, but to demonstrate that it is possible to estimate the optical quality of a site by numerical simulation of the aerodynamic field. Both the finite element formulation to compute the flow variables and the numerical strategy to compute the optical parameters have been described, the latter with some detail since, to our knowledge, such formulations have not been reported in the numerical literature.

There are of course many issues of our approach that could be debated. The reliability of the numerical results is essentially based on the capability of the *numerical implementation* of the LES model to really satisfy the design conditions (28) and (29). We have used the standard Smagorinsky LES model, with well known virtues and limitations. What we need in order to compute the structure constant of the temperature are the dissipations given by (27), and it is obvious that the *numerical dissipation will interact with the one provided by the LES model*. How important is this interaction is a point of discussion (see [23, 13]). In any case, changing the expression of the thermal and the mechanical dissipations would not alter our general approach.

As in most computational fluid dynamics simulations, even if the exact results computed have a limited validity, what is certainly reliable is the qualitative behavior predicted and the use of the numerical results for *comparison purposes*. In particular, we believe that the approach presented here is a valuable tool to compare the optical quality of different sites, for example to choose the location of a telescope facility as in the application we have presented.

Acknowledgments

The authors wish to thank the ATST team for providing the necessary information to simulate the ATST building at the Observatory of El Roque de los Muchachos, on the island of La Palma. J. Baiges would also like to acknowledge the support received from the *Departament d'Universitats, Recerca i Societat de la Informació* of the *Generalitat de Catalunya* (Catalan Government)

References

[1] ATST telescope: `http://atst.nso.edu/`.

[2] Y. Bazilevs, V.M. Calo, J.A. Cottrell, T.J.R. Hughes, A. Reali, and G. Scovazzi. Variational multiscale residual-based turbulence modeling for large eddy simulation of incompressible flows. *Computer Methods in Applied Mechanics and Engineering*, 197:173–201, 2007.

[3] J.M. Beckers. *Adaptive optics for astronomy: Principles, Perfomance and Applications*. Annual Reviews in Astronomy and Astrophysics, 1993.

[4] M. Cervera, R. Codina, and M. Galindo. On the computational efficiency and implementation of block-iterative algorithms for nonlinear coupled problems. *Engineering Computations*, 13(6):4–30, 1996.

[5] R. Codina. A nodal-based implementation of a stabilized finite element method for incompressible flow problems. *International Journal for Numerical Methods in Fluids*, 33:737–766, 2000.

[6] R. Codina. Stabilized finite element approximation of transient incompressible flows using orthogonal subscales. *Computer Methods in Applied Mechanics and Engineering*, 191:4295–4321, 2002.

[7] R. Codina and A. Folch. A stabilized finite element predictor–corrector scheme for the incompressible Navier–Stokes equations using a nodal based implementation. *International Journal for Numerical Methods in Fluids*, 44:483–503, 2004.

[8] R. Codina, J. Principe, O. Guasch, and S. Badia. Time dependent subscales in the stabilized finite element approximation of incompressible flow problems. *Computer Methods in Applied Mechanics and Engineering*, 196:2413–2430, 2007.

[9] C.E. Colosqui and A.A. Oberai. Generalized Smagorinsky model in physical space. *Computers & Fluids*, 37:207–217, 2008.

[10] ELT project: `http://www.eso.org/projects/e-elt/`.

[11] L.P. Franca and S.L. Frey. Stabilized finite element methods: II. The incompressible Navier-Stokes equations. *Computer Methods in Applied Mechanics and Engineering*, 99:209–233, 1992.

[12] GTC telescope: `http://www.gtc.iac.es/`.

[13] O. Guasch and R. Codina. A heuristic argument for the sole use of numerical stabilization with no physical LES modelling in the simulation of incompressible turbulent flows. Submitted.

[14] R.J. Hill. Structure functions and spectra of scalar quantities in the inertial-convective and viscous-convective ranges of turbulence. *Journal of the atmospheric sciences*, 46:2245–2251, 1989.

[15] T.J.R. Hughes. Multiscale phenomena: Green's function, the Dirichlet-to-Neumann formulation, subgrid scale models, bubbles and the origins of stabilized formulations. *Computer Methods in Applied Mechanics and Engineering*, 127:387–401, 1995.

[16] M.Z. Jacobson. *Fundamentals of Atmospheric Modeling*. Cambridge University Press, 2005.

[17] D.K. Lilly. The representation of small-scale turbulence theory in numerical simulation experiments. In H.H. Goldstine, editor, *Proc. IBM Scientific Computing Symp. on Environmental Sciences*, 1967.

[18] R. Löhner. *Applied CFD Techniques*. J. Wiley & Sons, 2001.

[19] L.J. Peltier and J.C. Wyngaard. Structure function parameters in the convective boundary layer from large eddy simulation. *Journal of the atmospheric sciences*, 52:3641–3660, 1995.

[20] S.B. Pope. *Turbulent Flows*. Cambridge University Press, 2000.

[21] C. Roddier and J. Vernin. Relative contribution of upper and lower atmosphere to integrated refractive-index profiles. *Applied optics*, 16:2252–2256, 1977.

[22] F. Roddier. *Adaptive optics in astronomy*. Cambridge University Press, 2004.

[23] P. Sagaut. *Large Eddy Simulation for Incompressible Flows*. Scientific Computing, Springer, 2001.

[24] V.I. Tatarski. *Wave propagation in a turbulent medium*. Dover Publications, INC, 1961.

[25] T.E. Tezduyar. Finite elements in fluids: Stabilized formulations and moving boundaries and interfaces. *Computers & Fluids*, 36:191–206, 2007.

[26] P. Venkatakrishnan and S. Chatterjee. On the saturation of the refractive index structure function–I. Enhanced hopes for long baseline optical interferometry. *Mon. Not. Royal Astronomical Society*, 224:265–269, 1987.

[27] L.P. Wang, S. Chen, and J.G. Brasseur. Examination of the hypothesis in the Kolmogorov refined turbulence theory through high resolution simulations. Part 2. Passive scalar fields. *Journal of Fluid Mechanics*, 400:163–197, 1999.